IEEE Access
Multidisciplinary ⋮ Rapid Review ⋮ Open Access Journal

Received 24 September 2023, accepted 25 October 2023, date of publication 30 October 2023,
date of current version 28 November 2023.

Digital Object Identifier 10.1109/ACCESS.2023.3328624

RESEARCH ARTICLE

Design and Evaluation of AX-Deminer Forearm Assistance for Demining Soldier

MYUNGHYUN LEE, YONGCHEOL KIM, GWANG TAE KIM, SANG HUN JOO, AND MAN BOK HONG

Ground Technology Research Institute, Agency for Defense Development, Daejeon 34060, South Korea

Corresponding author: Man Bok Hong (manbok.hong@gmail.com)

This work was supported by the Institute of the Civil Military Technology Cooperation funded by the Defense Acquisition Program Administration and Ministry of Trade, Industry and Energy of the Korean Government under Grant 19-CM-GU-01.

ABSTRACT Mine clearance operation using a mine detector often strains arm muscles because of the extended form of the detection pole. Implementing a gravity compensation device may be beneficial for alleviating this issue. Therefore, this paper presents a novel concept of passive-type forearm assistance for mine-detection soldiers. The proposed forearm assistance features a decoupled structure between a sweeping module and a gravity compensation unit. The sweeping module is implemented using a planar serial chain, allowing the required range of arm-sweeping motion for mine detection. The gravity compensation module, featuring a six-bar linkage with a linear spring, is located at the wearer's back and compensates the detector's weight transmitted through the sweeping module. The decoupled structure enables minimal exposure of the mechanism to the wearer. Design requirements are determined from motion analysis of mine-detection soldiers; kinematic relationships are derived for sweeping and gravity compensation modules. Based on the kinematic relationships, optimal synthesis methods are presented to determine design parameters. The proposed gravity compensation device has been experimentally validated for four mine-detection soldiers. Electromyography measurements of the upper limb demonstrate a significant reduction of up to 66% in % maximum voluntary contraction (MVC) when using forearm assistance. Thus, the proposed forearm assistance may reduce arm fatigue, enabling more extended operation duration during mine clearance tasks.

INDEX TERMS Forearm assistance, gravity compensation, mine detection, wearable device.

I. INTRODUCTION

After the domestic war of Korea, it is estimated that about two million landmines were buried at the demilitarized zone between North and South Korea [1]. Mine clearance is one of the critical issues that should be solved to prepare for reunification(or at least active inter-relations) between the two countries. One of the efforts is to aggressively clear mine by using mine clearance tanks that use tillers, rollers, flails, spikes, or a combination of these [2], [3], [4], [5], [6], [7], or autonomous robotic systems [8] including six-legged walking robots [9], [10], quadruped walking robots [11], two-wheel robots with a scanner [12], six-wheel robots with a scanner [13], and robots equipped with bogie mechanisms capable of traversing rough terrains [14]. Recently, the use of surveillance drones has been studied to detect landmines [15].

Most of the demilitarized zone of Korea is located in a mountainous area. The clearance of massive buried mines by exploding them may severely damage the ecological system. Finding the remains of soldiers killed during the war is also essential for clearing buried mines at the demilitarized zone. Consequently, the only possible solution so far is the manual clearance of mines by individual soldiers.

Demining soldiers perform their mission by holding and sweeping a mine-detection pole. For safe and accurate detection, it is required to sweep the pole steadily and slowly while keeping its sensor plate at a certain distance parallel to the ground. This procedure makes the arm muscles operating the pole get tired quickly. It restricts the operation time of demining, and it may be a potential risk to the soldier because muscle fatigue lowers the consentration level.

The associate editor coordinating the review of this manuscript and approving it for publication was Engang Tian.

We introduce in this paper a passive-type wearable device called Agency for defense development eXoskeleton (AX)—Deminer forearm assistance—to assist the weight of a mine-detection pole. It is based on a novel concept of a gravity compensation mechanism.

Various passive-type gravity compensation mechanisms have been developed to assist arm movements to assist individuals with insufficient arm strength or aiding workers in tasks requiring arm assistance. Devices that incorporate cam [16] or linkage structure [17] combined with springs have been reported to assist arm weight of users with diminished muscle strength. Some devices utilize simple parallelogram linkage structures to exclusively support the forearm [18], while others combine multiple link structures to independently support the weights of the forearm and upper arm [19]. Additionally, there are devices that utilize rubber bands to provide support for the arm weight [20]. These devices are primarily offered in configurations that are fixed to chairs, wheelchairs, or the floor due to considerations of size and weight. However, devices intended to aid workers in tasks involving their arms are typically designed in a wearable form, ensuring both ease of use and adaptability across diverse work settings.

Various research efforts have been dedicated to developing devices that aid workers in their tasks [21], [22], [23]. Notably, commercial products like PAEXO (Ottobock, Duderstadt, Germany) [24], Ekso EVO (Ekso Bionics®, Richmond, CA, USA) [25], and the Airframe™(Levitate Technologies, San Diego, CA, USA) [26] have been employed to assist workers. These devices predominantly employ simple forms of gravity compensation mechanisms using levers and elastic elements to support workers [27]. However, these mechanisms primarily cater to overhead tasks and upper arm assistance, often falling short in fully compensating for loads experienced by the forearm and wrist regions when dealing with heavy equipments. On the other hand, devices such as EXHAUSS stronger [28], Robomate [29], [30], Lockheed FORTIS [31], are designed to aid workers handling heavy tools. Moreover, an assistive device for hand held cameras were reported [32]. These devices typically are operated based on parallelogram-based gravity compensation schemes with integrated springs. They are attached to the end of the arm, wrist, or hand, providing support against the loads encountered during arm motions. Consequently, the construction of these devices requires incorporating gravity compensation units that consider the arm's range of motion, leading to a significant increase in device size. A device proposed in [33] adopts a different approach by providing load assistance at the end of the arm while positioning the gravity compensation unit on the user's back. However, this device presents a challenge in that the force-transmitting pantograph structure is aligned with the arm, potentially limiting arm movement or causing interference during operation.

Kineto-elastic chains of most passive-type gravity compensation mechanisms are composed of linkages to generate the required motions and springs embedded into the motion generation linkages. Because of the coupled nature of the motion generation linkages and gravity compensation units, it is difficult to make the size of the overall mechanism slim. The demining process performed by a soldier requires high concentration and delicate movement of the soldier. Consequently, minimizmg mechanical components of the motion generation linkage for compact size with light weight is desirable to avoid unintentional interference caused by moving parts of the mechanism.

For this purpose, the proposed forearm assistance has been designed to decouple the motion generation unit from the gravity compensation part. Gravity compensation module is located at the back of the wearer; a simple serial chain is only exposed at the side of the wearer as a sweeping module. Because of the decoupled approach, moving parts that may interfere with the soldier's movements can be minimized.

Design requirements are analyzed in Section II. The structural overview and the analysis of the kinematic and kinetic relationship of each module (sweeping module and gravity compensation module) are presented in Section III. In Section IV, the kinematic structure of each module is synthesized by parameter optimization, and the prototype design of the proposed forearm assistance is introduced. Finally, the performance evaluation is presented in Section V based on experiments against four training assistants for mine detection.

II. DESIGN REQUIREMENTS

Mine detecting motions were captured and analyzed to design the proposed forearm assistance. Two soldiers participated in this experiment. One of them is a demining instructor; the other is a soldier who performs real demining missions in the demilitarized zone of Korea. The mine-detection operations were performed for four environmental conditions(Fig. 1). They performed the following prescribed pattern of the mine-detection operation. First, sweep the pole from left to right; move one half-step forward. Second, sweep back from right to left; then, move one half-step forward again. Repeat this procedure for three cycles.

Both are right-handed; thus, the operating range of the forearm assistance was determined by the range of motion of the right hand. Motion data of upper extremities were measured using an inertial measurement unit(IMU)-based motion capture suit (MVN Link, Movella, US). The motion data were sampled with 240 Hz and filtered by the zero-phase fifth-order Butterworth low-pass filter with a cutoff frequency of 15 Hz [34]. For accurate comparisons across different environments, each data cycle was equally segmented and arranged from the position initiating the sweeping motion from the left to the position returning to the left again.

We determined the range of motion of the right hand by evaluating the three-dimensional motion data with respect to the coordinates located at the center of the pelvis. The X- and Y- axes of the coordinates were chosen along the forward and left directions of the body.

FIGURE 1. Deming motion performed by trained soldiers at four different environment conditions: (a) indoor level ground, (b) outdoor uphill, (c) outdoor downhill, and (d) outdoor level ground.

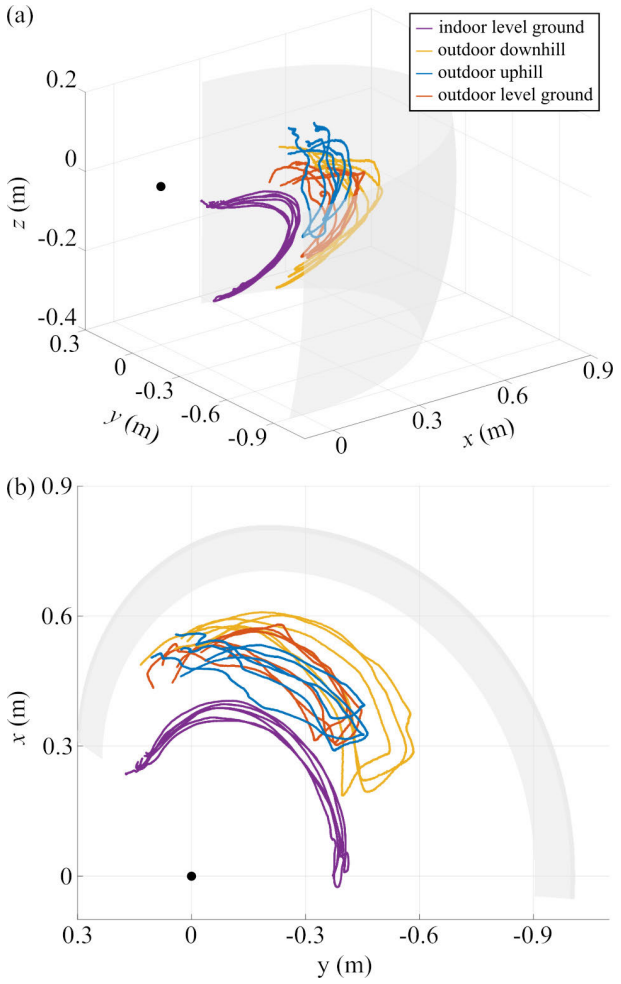

FIGURE 2. Motion trajectories of right hand and the achievable workspace of the designed sweeping module. The graph is displayed in a local pelvic coordinate system at the pelvic center (black dot), depicting trajectories of the right hand for indoor level ground (purple), outdoor downhill (yellow), outdoor uphill(blue), and outdoor level ground with rocks (red) conditions. The achievable workspace of the designed sweeping module is illustrated as the gray surface: (a) Isometric view and (b) top view.

The captured motion trajectories are depicted in Fig. 2. The range of motion was quantified using the spherical coordinate system. If we let $\boldsymbol{p}$ be a point of the right hand, it can be expressed as $\boldsymbol{p} = [r, \theta, \phi]$, where r denotes distance to the right hand from the center of the pelvis. Elevation angle, ϕ, is the angle between $\boldsymbol{p}$ and its orthogonal projection onto the XY- plane; azimuth angle, θ, is defined as the angle between the X- axis and the orthogonal projection of $\boldsymbol{p}$ onto the XY- plane.

The range of motion of the right hand was determined by the maximum and minimum values (Table 1). The mean of the maximum (and minimum) values of each trial are also presented in the Table 1.

Referring to Table 1, the range of distance r is estimated from 310 to 677 mm. The min. (and max.) value of r for indoor level ground was smaller than r min. (and r max.) of the other conditions. Even the mean of r max. obtained from the indoor level ground was smaller than the mean values of r min. from the other outdoor cases. In contrast, the longest of arm reach was observed while detecting at the downhill slope. Furthermore, the operations at outdoor uphill and level ground require a similar range of movement of arm reach, r.

The range of sweeping motion, azimuth angle θ, is expected to be $-90.8° \leq \theta \leq 32.2°$ (Table 1). A negative (or positive) value of θ implies sweeping the pole to the right (or left) side of the body. The widest range of sweeping motion was observed while sweeping at indoor level ground. While the mean values of θ max. for three outdoor cases are similar, the mean of θ min. for downhill operation is smaller than those of the other outdoor conditions, uphill and level ground. This finding implies that the sweeping angle toward the left was similar for outdoor cases. However, for sweeping toward the right, a larger sweeping range was seen for the downhill operation than in the other two cases.

The elevation of the detection pole was estimated by the movement range of elevation angle, $-28.6° \leq \phi \leq 3.0°$ (Table 1). ϕ max. is negative for most working conditions except uphill operation, which indicates that during mine detection, the right-hand position is located under the center of the pelvis but for the operation at the uphill slope, the right hand was lifted over the center of the pelvis up to 3 degrees. Furthermore, the elevation of the hand position for the downhill case is similar to the range for outdoor level ground.

During the motion acquisition experiments, the mass property of the mine-detection pole currently used by Korean soldiers was also analyzed. The total mass of the detection pole is 4.45 kg. The mass center is located closely under the hand grip; the variation in the mass center with respect to the change in length of the detection pole is minimal

TABLE 1. Range of motion of demining operation: Variation of hand position, $p = [r, \theta, \phi]$.

Environments		Distance, r (mm)				Azimuth angle, θ (deg)				Elevation angle, ϕ (deg)			
		min	mean	max	mean	min	mean	max	mean	min	mean	max	mean
Indoor	Level Ground	308	310 ± 2	456	449 ± 9	-93.8	-90.8 ± 2.7	36.2	32.2 ± 3.5	-29.6	-28.6 ± 1.5	-12.7	-13.6 ± 1.0
Outdoor	Downhill	489	506 ± 17	695	677 ± 22	-67.3	-65.9 ± 1.4	15.3	7.1 ± 7.4	-26.5	-21.6 ± 4.3	-1.0	-3.2 ± 2.24
	Uphill	435	473 ± 33	603	580 ± 20	-55.2	-52.8 ± 3.2	11.8	6.3 ± 4.8	-13.7	-12.3 ± 2.1	4.6	3.0 ± 1.4
	Level Ground	457	467 ± 15	628	615 ± 11	-52.6	-50.5 ± 2.3	14.0	10.2 ± 3.3	-21.8	-20.1 ± 1.5	-3.6	-4.3 ± 0.7

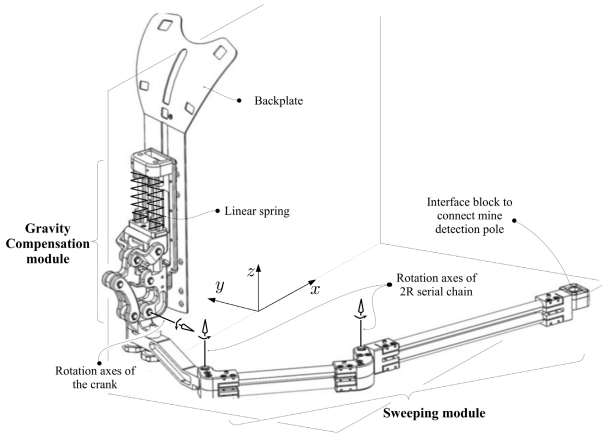

FIGURE 3. Structural overview of AX-Deminer forearm assistance.

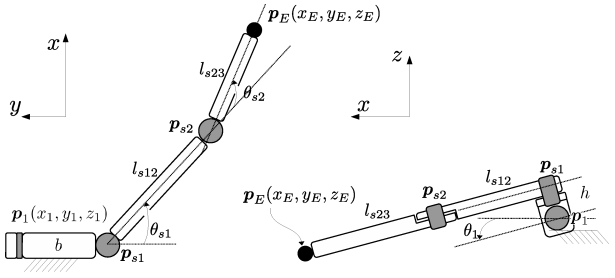

FIGURE 4. Kinematic structure and parameters of the sweeping module.

(around 35 mm) relative to the total length of the pole. Thus, it is assumed that the target mass for gravity compensation is 4.45 kg, located at the hand grip (or right-hand position).

III. KINEMATIC ANALYSIS

A. KINEMATIC STRUCTURE

The structural overview of the proposed forearm assistance is depicted in Fig. 3. The proposed forearm assistance comprises two decoupled mechanisms, sweeping and gravity compensation modules. The sweeping module comprises two-degrees-of-freedom (2-DOF) planar serial chain whose joints are passive revolute pairs. An interface exists at the end-tip of the serial chain such that the mine-detection pole can be connected to the end-tip through a ball joint at the interface block. Because of this kinematic structure, the detection pole has 2-DOF spherical wrist motion with 3-DOF planar movement with respect to the base of the serial chain.

The gravity compensation module was designed based on a six-bar linkage comprising a crank-slider linkage with one revolute-revolute (RR) dyad. A linear spring lies between the base and slider block. Thus, when an external torque is acted on the crank of the six-bar, resistive torque is generated by the compression force of the linear spring.

The base of the sweeping module is attached to the crank of the six-bar linkage of the gravity compensation module. The proposed forearm assistance was designed such that the motion plane of the six-bar linkage is perpendicular to that of the serial chain implying that the rotation axis of the crank is perpendicular to the joint rotation axes of the serial chain. Thus, an external load imposed at the end-tip of the serial chain results in rigid rotation of the serial chain with respect to the rotation axis of the crank. However, the rotation of the crank is resisted by the compensational force of the linear spring through the six-bar structure of the gravity compensation module.

The ground of the proposed forearm assistance is rigidly attached to the backplate; thus, all parts of the gravity compensation module are located at the back of the wearer. A passive serial arm with a simple structure is only exposed to the workspace of the mine-detection soldier. This decoupled structure is expected to enhance wearability and minimize mechanical interference during a high-concentration task.

B. SWEEPING MODULE

The sweeping module is achieved using a 2R serial chain. The purpose of the kinematic analysis is to find two joint angles of the 2R serial chain and the input crank angle of six-bar linkage of the gravity compensation module, when end-tip position $\boldsymbol{p}_E(x_E, y_E, z_E)$ is given. Because the base of the 2R serial chain is attached to the crank of the six-bar linkage, crank angle is also considered here for the inverse kinematic analysis of the sweeping module.

The kinematic structure is depicted in Fig. 4. Two revolute pairs of the 2R serial chain are denoted as $\boldsymbol{p}_{s1}$ and $\boldsymbol{p}_{s2}$. The revolute joint of the crank of the six-bar linkage is represented as $\boldsymbol{p}_1$. The rotation axis of $\boldsymbol{p}_1$ is prependicular to those of $\boldsymbol{p}_{si}$ (for $i = 1, 2$). Link length between $\boldsymbol{p}_{s1}$ and $\boldsymbol{p}_{s2}$ (or $\boldsymbol{p}_{s2}$ and $\boldsymbol{p}_E$) is expressed as l_{s12} (or l_{s23}). Furthermore, the joint angle of $\boldsymbol{p}_{si}$ is represented as θ_{si}; the crank angle of the six-bar linkage is expressed as θ_1.

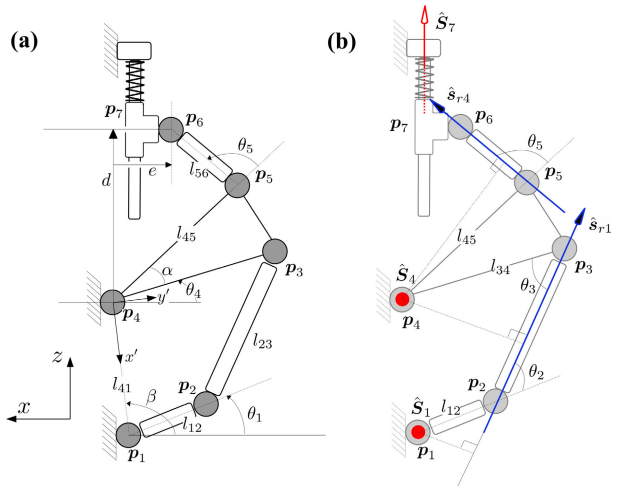

FIGURE 5. Kinematic structure of the gravity compensation module. Figure (a) illustrates parameters for the kinematic analysis of the module; screws for the force analysis are represented in Fig (b). Screw $\hat{S}_i$ denotes joint screw of the i-th joint. $\hat{S}_i$ except $\hat{S}_7$ is a line passing through p_i and has the direction along the $y-$ axis. Joint screw $\hat{S}_7$ is a free vector having the direction along the $z-$ axis. Reciprocal screw $\hat{s}_{r1}$ (or $\hat{s}_{r4}$) implies the screw reciprocal to $\hat{S}_2$ and $\hat{S}_3$ except $\hat{S}_1$ (or reciprocal to $\hat{S}_5$ and $\hat{S}_6$ except $\hat{S}_4$).

The end-tip position $\boldsymbol{p}_E$ is estimated from the trace of the wearer's hand position during the mine detection. Referring to Fig. 4, the following kinematic relationship can be obtained:

$$x_E - x_1 = h s_{\theta_1} + c_{\theta_1}(l_{s12}s_{\theta_{s1}} + l_{s23}s_{\theta_{s1}+\theta_{s2}}), \tag{1a}$$
$$y_E - y_1 = -b - (l_{s12}c_{\theta_{s1}} + l_{s23}c_{\theta_{s1}+\theta_{s2}}), \text{ and} \tag{1b}$$
$$z_E - z_1 = h c_{\theta_1} - s_{\theta_1}(l_{s12}s_{\theta_{s1}} + l_{s23}s_{\theta_{s1}+\theta_{s2}}), \tag{1c}$$

where symbols c and s are used to denote cosine and sine functions; b and h are joint offsets between $\boldsymbol{p}_1$ and $\boldsymbol{p}_{s1}$ (Fig. 4). From (1a) and (1c), θ_1 is obtained as follows:

$$\theta_1 = 2\tan^{-1}\frac{B \pm \sqrt{A^2 + B^2 - h^2}}{A + h}, \tag{2}$$

where $A \equiv z_E - z_1$ and $B \equiv x_E - x_1$. Because we know θ_1, joint angles of the 2R serial chain, θ_{s1} and θ_{s2}, can be found from (1a) and (1b). Rearranging the two equations yields

$$l_{s12}s_{\theta_{s1}} + l_{s23}s_{\theta_{s1}+\theta_{s2}} = C \quad \text{and}$$
$$l_{s12}c_{\theta_{s1}} + l_{s23}c_{\theta_{s1}+\theta_{s2}} = D, \tag{3}$$

where $C \equiv (1/c_{\theta_1})(x_E - x_1) - (s_{\theta_1}/c_{\theta_1})h$ and $D \equiv b - (y_E - y_1)$. From (3), θ_{s2} is determined by eliminating θ_{s1}.

$$\theta_{s2} = \cos^{-1}\frac{C^2 + D^2 - l_{s12}^2 - l_{s23}^2}{2 l_{s12} l_{s23}}. \tag{4}$$

The remaining joint angle θ_{s1} of the 2R serial chain is then found from (4) and (3).

C. GRAVITY COMPENSATION MODULE

The kinematic structure of the gravity compensation module is depicted in Fig. 5. It is based on the crank-slider linkage such that compensation torque can be acted on the revolute joint of the driven crank, $\boldsymbol{p}_1$ by the compressive force of a linear spring. However, the kinematic structure of the crank-slider linkage does not have enough design parameters to achieve the required torque profile. Thus, a six-bar structure is implemented to passively generate the compensation module.

When end-tip position $\boldsymbol{p}_E$ is given, the required rotation angle of the driven crank, θ_1, is obtained from (2). The kinematic analysis of the gravity compensation module is to find the linear displacement of the slider block, d, for the given rotation angle of the driven crank, θ_1. Joints of the six-bar linkage are expressed as $\boldsymbol{p}_i$ (for $i = 1, 2, \cdots, 7$); link length between $\boldsymbol{p}_i$ and $\boldsymbol{p}_j$ is represented by l_{ij} (Fig. 5).

The kinematic relationship of inner 4-bar linkage formed by $\boldsymbol{p}_i$ (for $i = 1, 2, 3, 4$) can be formulated from the following constraint:

$$(\boldsymbol{p}_3 - \boldsymbol{p}_2)\cdot(\boldsymbol{p}_3 - \boldsymbol{p}_2) = l_{23}^2. \tag{5}$$

If the local coordinate frames $\boldsymbol{p}_4 - x'y'z'$ depicted in Fig. 5 are considered, $\boldsymbol{p}_3$ and $\boldsymbol{p}_2$ can be written as,

$$\boldsymbol{p}_3 = l_{34}[\cos(\pi - \beta + \theta_4), \sin(\pi - \beta + \theta_4)]^T \quad \text{and}$$
$$\boldsymbol{p}_2 = [l_{41} + l_{12}\cos(\pi - \beta + \theta_1), l_{12}\sin(\pi - \beta + \theta_1)]^T, \tag{6}$$

where β is the angle between $x-$ and $x'-$ axes. Substituting (6) into (5) and rearranging the result with respect to θ_4 yields

$$E\cos(\theta_4') + F\sin(\theta_4') = G, \tag{7}$$

where

$$\begin{cases} E &= 2\, l_{34}(l_{41} + l_{12}\cos\theta_1') \\ F &= 2\, l_{12} l_{34}\sin\theta_1' \\ G &= l_{12}^2 + l_{34}^2 + l_{41}^2 - l_{23}^2 + 2 l_{12} l_{41}\cos\theta_1'. \end{cases}$$

In the above equations, θ_1' and θ_4' are defined as $\theta_i' = \pi - \beta + \theta_i$ (for $i = 1, 4$). The output angle of the driven crank, θ_4 is determined by solving (7) as follows:

$$\theta_4 = -\pi + \beta + 2\tan^{-1}\frac{F \pm \sqrt{E^2 + F^2 - G^2}}{E + G}. \tag{8}$$

We now consider the inner crank-slider which is formed by $\boldsymbol{p}_4, \boldsymbol{p}_5, \boldsymbol{p}_6$, and $\boldsymbol{p}_7$. The following kinematic relationships can be formulated:

$$\begin{cases} l_{45}\sin(\alpha + \theta_4) + l_{56}\sin(\alpha + \theta_4 + \theta_5) = d \\ l_{45}\cos(\alpha + \theta_4) + l_{56}\cos(\alpha + \theta_4 + \theta_5) = e, \end{cases} \tag{9}$$

where α implies the angle between l_{34} and l_{45}; symbols d and e are offset distances of $\boldsymbol{p}_6$ relative to $\boldsymbol{p}_4$ along the $z-$ and $x-$ axes. If two equations of (9) are substituted into the trigonometric identity, $\sin^2(\alpha+\theta_4+\theta_5)+\cos^2(\alpha+\theta_4+\theta_5) = 1$, the displacement of linear spring, d, is obtained as follows:

$$d = l_{45}\sin(\alpha + \theta_4) \pm \sqrt{H}, \tag{10}$$

where $H \equiv -l_{45}^2\cos^2(\alpha + \theta_4) - e^2 + l_{56}^2 + 2 e l_{45}\cos(\alpha + \theta_4)$.

D. FORCE/TORQUE TRANSMISSION

After the kinematic analysis of the gravity compensation module was performed, all joint positions $\boldsymbol{p}_i$ (for $i = 1, 2, \cdots, 7$) are determined. Then, joint torque at $\boldsymbol{p}_1$ induced by the spring compression can be formulated using joint screws and their reciprocal ones.

We first consider the inner four-bar linkage formed by $\boldsymbol{p}_i$ (for $i = 1, 2, 3, 4$). The twist of output link l_{34} can be formulated as

$$\hat{\boldsymbol{T}}_{l_{34}} = \omega_4 \hat{\boldsymbol{S}}_4 = \omega_1 \hat{\boldsymbol{S}}_1 + \omega_2 \hat{\boldsymbol{S}}_2 + \omega_3 \hat{\boldsymbol{S}}_3, \tag{11}$$

where ω_i denotes the angular velocity of joint $\boldsymbol{p}_i$. The rotation axis of revolute pair, $\boldsymbol{p}_i$ is expressed as a unit screw with zero pitch, $\hat{\boldsymbol{S}}_i$; it is a line passing through $\boldsymbol{p}_i$ and having the direction along the $y-$ axis. Let $\hat{\boldsymbol{s}}_{r1}$ be the unit reciprocal screw which is reciprocal to $\hat{\boldsymbol{S}}_2$ and $\hat{\boldsymbol{S}}_3$ except $\hat{\boldsymbol{S}}_1$. As depicted in Fig. 5(b), $\hat{\boldsymbol{s}}_{r1}$ becomes a line passing through $\boldsymbol{p}_2$ and $\boldsymbol{p}_3$ and lying on the xz- plane. Using $\hat{\boldsymbol{s}}_{r1}$, we have the following relationship from (11):

$$\omega_4 = (\hat{\boldsymbol{s}}_{r1}^T \hat{\boldsymbol{S}}_1 / \hat{\boldsymbol{s}}_{r1}^T \hat{\boldsymbol{S}}_4)\omega_1, \tag{12}$$

where $\hat{\boldsymbol{s}}_{r1}^T \hat{\boldsymbol{S}}_j$ is the reciprocal product of two screws, because $\hat{\boldsymbol{s}}_{r1}$ and $\hat{\boldsymbol{S}}_j$ are expressed as the Plücker's ray and axis coordinates [35].

We now consider inner crank-slider linkage which is formed by $\boldsymbol{p}_i$ (for $i = 4, 5, \cdots, 7$). In the similar manner as we used for (12), velocity relationship between revolute joint $\boldsymbol{p}_4$ and sliding pair $\boldsymbol{p}_7$ can be obtained as

$$v_7 = (\hat{\boldsymbol{s}}_{r4}^T \hat{\boldsymbol{S}}_4 / \hat{\boldsymbol{s}}_{r4}^T \hat{\boldsymbol{S}}_7)\omega_4. \tag{13}$$

In the above equation, the linear velocity of sliding block is expressed as v_7; unit screw $\hat{\boldsymbol{s}}_{r4}$ is the unit line vector which is reciprocal to $\hat{\boldsymbol{S}}_5$ and $\hat{\boldsymbol{S}}_6$ except $\hat{\boldsymbol{S}}_4$. It is expressed with the Plucker's ray coordinates; geometrically, it is the line passing through $\boldsymbol{p}_5$ and $\boldsymbol{p}_6$ and lying on the xz- plane.

From (12) and (13), the input and output velocity relationship between ω_1 and v_7 can be determined. If torque input imposed at $\boldsymbol{p}_1$ is represented by τ_1, the resistive force f_7 which is acted by the linear spring can be found from the virtual work principle, $\omega_1 \tau_1 = v_7 f_7$,

$$f_7 = \frac{(\hat{\boldsymbol{s}}_{r4}^T \hat{\boldsymbol{S}}_7)(\hat{\boldsymbol{s}}_{r1}^T \hat{\boldsymbol{S}}_4)}{(\hat{\boldsymbol{s}}_{r4}^T \hat{\boldsymbol{S}}_4)(\hat{\boldsymbol{s}}_{r1}^T \hat{\boldsymbol{S}}_1)} \tau_1. \tag{14}$$

Because the rotation axis $\hat{\boldsymbol{S}}_i (\in \boldsymbol{R}^{6\times1})$ of revolute pair $\boldsymbol{p}_i$ (for $i = 1, 2, \cdots 6$) is expressed as the Plücker's axis coordinate, it can be written as $\hat{\boldsymbol{S}}_i = \left[(\boldsymbol{p}_i \times \boldsymbol{s}_i)^T, \boldsymbol{s}_i^T\right]^T$, where $\boldsymbol{s}_i (\in \boldsymbol{R}^{3\times1})$ is a unit direction vector along the axis; $\boldsymbol{p}_i (\in \boldsymbol{R}^{3\times1})$ is a position vector to the center of the i-th revolute pair. The screw for the prismatic pair $\hat{\boldsymbol{S}}_7$ can be written as $\hat{\boldsymbol{S}}_7 = \left[\boldsymbol{s}_7^T, \boldsymbol{0}_{3\times1}^T\right]^T$, because the joint screw of prismatic pair is a free vector (screw with infinite pitch). Reciprocal screw $\hat{\boldsymbol{s}}_{rj} (\in \boldsymbol{R}^{6\times1})$ (for $j = 1, 4$) is expressed as Plücker's ray coordinate. Thus, it can be written as $\hat{\boldsymbol{s}}_{rj} = \left[\boldsymbol{s}_{rj}^T, (\boldsymbol{r}_{rj} \times \boldsymbol{s}_{rj})^T\right]^T$, where $\boldsymbol{s}_{rj} (\in \boldsymbol{R}^{3\times1})$ is a unit direction vector along the axis of $\hat{\boldsymbol{s}}_{rj}$, and a position vector $\boldsymbol{r}_{rj}$ to a point along $\hat{\boldsymbol{s}}_{rj}$ can be found as $\boldsymbol{r}_{r1} = \boldsymbol{p}_2$ and $\boldsymbol{r}_{r2} = \boldsymbol{p}_5$. Because all joint position vectors $\boldsymbol{p}_i$'s are found from the kinematic analysis, the force/torque transmission between τ_1 and f_7 can be computed from (14).

Geometrically, the reciprocal product of two unit lines becomes the perpendicular distance between the two lines; the reciprocal product of a line and a free vector is expressed as inner product between direction vectors of them. Thus, (14) can be written as

$$f_7 = \frac{l_{34} \sin(\theta_3) \sin(\theta_4 + \theta_5 + \alpha)}{l_{12} l_{45} \sin(\theta_2) \sin(\theta_5)} \cdot \tau_1. \tag{15}$$

In the above equation, θ_2 (or θ_3) is the angle between $(\boldsymbol{p}_2 - \boldsymbol{p}_1)$ and $(\boldsymbol{p}_3 - \boldsymbol{p}_2)$ (or $(\boldsymbol{p}_3 - \boldsymbol{p}_2)$ and $(\boldsymbol{p}_3 - \boldsymbol{p}_4)$). Since we know all joint position vectors $\boldsymbol{p}_i$'s from the kinematic analysis, θ_2 and θ_3 can be found as follows:

$$\theta_2 = \cos^{-1} \frac{(\boldsymbol{p}_2 - \boldsymbol{p}_1) \cdot (\boldsymbol{p}_3 - \boldsymbol{p}_2)}{l_{12} l_{23}},$$

and

$$\theta_3 = \cos^{-1} \frac{(\boldsymbol{p}_3 - \boldsymbol{p}_2) \cdot (\boldsymbol{p}_3 - \boldsymbol{p}_4)}{l_{23} l_{34}}.$$

IV. DESIGN

A. PARAMETER OPTIMIZATION

1) SWEEPING MODULE

Referring to Fig. 4, parameters to be determined for the sweeping module are the position of the first joint, $\boldsymbol{p}_{s1} = (x_{s1}, y_{s1}, z_{s1})$ and two link lengths, l_{s1} and l_{s2}. The sweeping module must have a reachable workspace embracing the desired range of motion depicted in Fig. 2.

The sweeping module is the only moving element that follows a large sweeping motion of the wearer. For wearability and manipulability, the kinematic parameters of the mechanism were optimized to minimize the weights of moving bodies. If it is assumed that two bodies l_{s12} and l_{s23} are manufactured with the same material having the same cross-sectional area, the total weight of the sweeping module is proportional to $l_{s12} + l_{s23}$. The objective for optimization is as follows:

$$\begin{cases} \textit{Minimize}: & F_s(l_{s12}, l_{s23}) = \alpha l_{s12} + l_{s23} \\ \textit{Subject to}: & V_s \supset V_{req}, \end{cases} \tag{16}$$

where $\alpha = 1.5$ is a weighting factor for l_{s12}; V_{req} and V_s are the required and optimized range of motion of the sweeping module. It is desirable to shorten the link, l_{s12}, close to the base for sufficient rigidity of the serial arm under bending conditions. Thus, weighted link length αl_{s12} is used for the optimization. The range of motion of the sweeping module's end point, determined by the optimized link lengths, is depicted as a gray surface in Fig. 2. The optimization process was resolved by fmincon function of MATLAB R2019b program. In order to avoid interference between the wearer's body and the first link of sweeping module, l_{s12}, the distance to $\boldsymbol{p}_{s2}$ is constrained such that it is greater than 250 mm during the optimization. In addition,

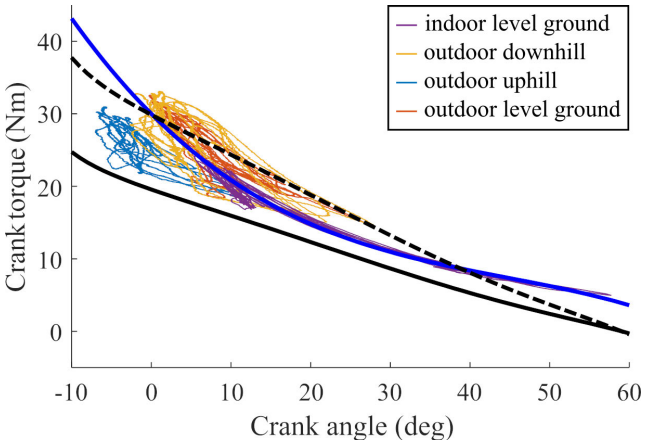

FIGURE 6. Torque loads imposed at the crank of the gravity compensation module from mine detector's weight. Among the torque profiles of four environment conditions (thin solid lines), the torque profile at indoor working conditions was used as the reference torque profile for the design. The thick solid line with blue color denotes the reference load profile fitted with the third-order polynomial. The load profile that can be achieved by the optimized gravity compensation module is represented by the black-dashed line. For the prototype design, stiffness coefficient of the linear spring was changed from optimized value, 9,215.7 N/m to 6,040 N/m. The load profile for the prototype is expressed as a thick solid line with black color.

link lengths are bound to be 100 mm $< l_{s12}, l_{s23} <$ 800 mm for reasonable and compact realization of sweeping module.

2) GRAVITY COMPENSATION MODULE

In Section II, it was assumed that the mass for compensation is 4.45 kg and the mass center is located at the handle of the detection pole. The detection pole is connected to the end effector of the sweeping module at $\boldsymbol{p}_E$. Because the connection point is located at the bottom of the handle of the detection pole, we further assume that the weight of the detection pole is acted at $\boldsymbol{p}_E$. The moment $\tau_{1,\text{load}}$, caused by the detection pole, acting at the revolute pair $\boldsymbol{p}_1$ is computed as

$$\tau_{1,\text{load}} = -mg\boldsymbol{k} \times (\boldsymbol{p}_E - \boldsymbol{p}_1) \cdot \boldsymbol{j}, \tag{17}$$

where m is the mass of the mine detector; vectors $\boldsymbol{k}$ and $\boldsymbol{j}$ imply unit vectors along the $z-$ and $y-$ axes. Required path of $\boldsymbol{p}_E$ was obtained from Section II. For the given $\boldsymbol{p}_E$, the corresponding crank angle of six-bar θ_1 is found from (2); the torque imposed at the crank is computed from (17). Thus, the torque load that should be compensated at each crank angle can be obtained as depicted in Fig. 6. Considering the base coordinates depicted in Figs. 4 and 5, positive rotation of the crank implies lowering the detection pole. While the detection pole is lowered by up to 60 degrees of the crank rotation during the indoor experiment, the range of rotation required at the real outdoor field is limited to $-10° \leq \theta_1 \leq 30°$. The detection pole is raised up to 10 degrees of the crank rotation for the uphill operating condition. Based on data from the indoor operation, the reference load profile for the design of the gravity compensation module is determined as follows:

$$\tau_{1,\text{load}}(\text{Nm}) = -0.00015\theta_1^3 + 0.02\theta_1^2 - 1.1\theta_1 + 30.0, \tag{18}$$

where θ_1 is expressed in degrees. The fitted load profile is depicted as a blue line in Fig. 6.

Let k be the stiffness of the linear spring. When the crank of the six-bar linkage is rotated to θ_1, a resistive torque is acted on the crank caused by the deflection of the linear spring. If we let $\tau_{1,\text{spring}}$ be the resistive torque acted on the crank by the linear spring, it can be computed using (14).

$$\tau_{1,\text{spring}} = -k\frac{(\hat{\boldsymbol{s}}_{r4}^T\hat{\boldsymbol{S}}_4)(\hat{\boldsymbol{s}}_{r1}^T\hat{\boldsymbol{S}}_1)}{(\hat{\boldsymbol{s}}_{r4}^T\hat{\boldsymbol{S}}_7)(\hat{\boldsymbol{s}}_{r1}^T\hat{\boldsymbol{S}}_4)}(d - d_0), \tag{19}$$

where d_0 denotes the initial offset along the $z-$axis of $\boldsymbol{p}_6$ relative to $\boldsymbol{p}_4$; thus, $d - d_0$ is the amount of spring deflection. Parameter optimization aims to minimize the energy difference between the potential energy given by the spring and the desired energy to compensate for the detection pole.

$$Minimize: F_G(\boldsymbol{X}) = \int_{\theta_{1,min}}^{\theta_{1,max}} |\tau_{1,\text{spring}} - \tau_{1,\text{load}}| d\theta_1 \tag{20}$$

where $\boldsymbol{X}$ denotes the vector of design variables, $\boldsymbol{X} = [\alpha, \beta, h, l_0, l_1, \cdots, l_5, k, d_0]$.

The parameters of the gravity compensation module were determined by optimization. The optimization process was performed using fmincon function of MATLAB R2019b program. Constraints for the optimization are lower and upper bounds of each design variables; each bound was set by considering physical feasibility. The load profile that can be achieved by the optimized gravity compensation module is depicted in Fig. 6 as a black-dashed line. The maximum deviation between the reference (blue line) and the achievable torque profile (black-dashed line) is 5.4 Nm at $\theta_1 = -10°$.

B. PROTOTYPE DESIGN

Based on the results of parameter optimization, the prototype of the forearm assistance was designed as depicted in Fig. 7. Most links were manufactured with aluminum alloy,

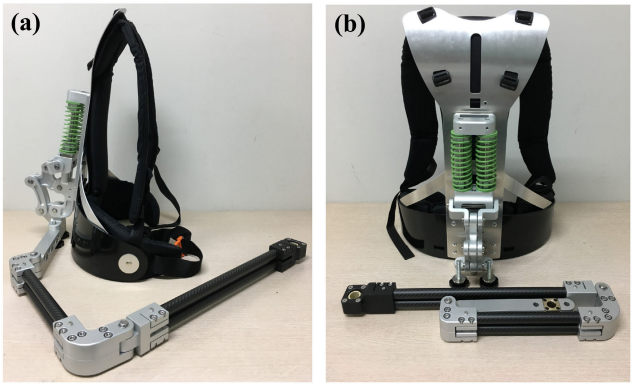

FIGURE 7. Prototype of AX-Deminer forearm assistance.

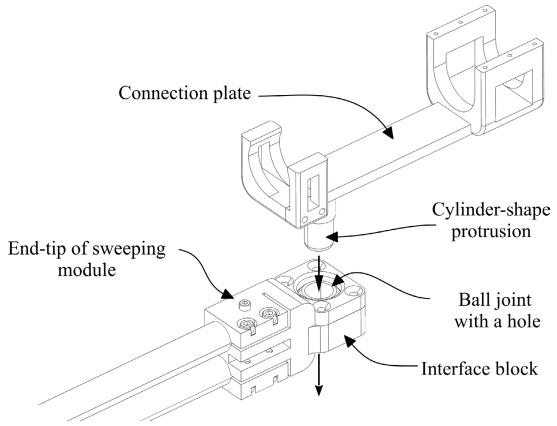

FIGURE 8. Interface between the sweeping module and mine-detection pole. The interface block at the end-tip contains a ball joint with a hole. Connection plate is attached at the bottom of mine-detection pole. Mine-detection pole is connected to the end-tip by inserting the cylinder-shaped protrusion of the connection plate into the hole at the ball joint. This structure enables 3-DOF rotations of the mine-detection pole with respect to the end-tip of the sweeping module.

TABLE 2. Conditions and parameters of finite element analysis simulation.

Conditions and parameters	Values
Mesh type	Solid mesh
Meshing option	Standard mesher
Automatic transition	Clear
Jacobian points	16
Element size (mm)	5
Tolerance (mm)	0.25
Mesh quality	High quality
Number of nodes	135924
Number of elements	71669
Maximum aspect ratio	52.927
Percentage of elements with an aspect ratio less than 3 (%)	79.9
Percentage of elements with an aspect ratio greater than 10 (%)	0.64
Number of elements	71669
Maximum aspect ratio	52.927

Al-6061 T6. However, two links, l_{s12} and l_{s23} of the sweeping module were achieved using a carbon fiber hollow shaft to reduce the weight of the moving parts. The total weight of the prototype device is 5.7 kg.

The sweeping module trasmits payload weight to the gravity compensation module; thus, the rigidity of the serial arm is vital for the proper operation of the gravity compensation module. Considering both the rigidity and weight of the serial arm, a finite element analysis (FEA) was conducted to tune the dimensions and material of the serial arm. The FEA was simulated in SOLIDWORKS® 2021 (Dassault Systèmes, France). Revolute pair, p_{s1}, has been subjected to a fixed hinge restraint, and the two linkages have been set to be bonded at the revolute pair, p_{s2}. A 50 N load was applied vertically downward on the upper surface of the end-effector's interface block (Fig. 8). Detailed information about the simulation was presented in Table. 2. The result is depicted in Fig. 9. For 50 N of payload weight, 0.69 mm of end-tip deflection of the sweeping module is expected at full-stretch configuration. The factor of safety is calculated as 1.8 from this analysis.

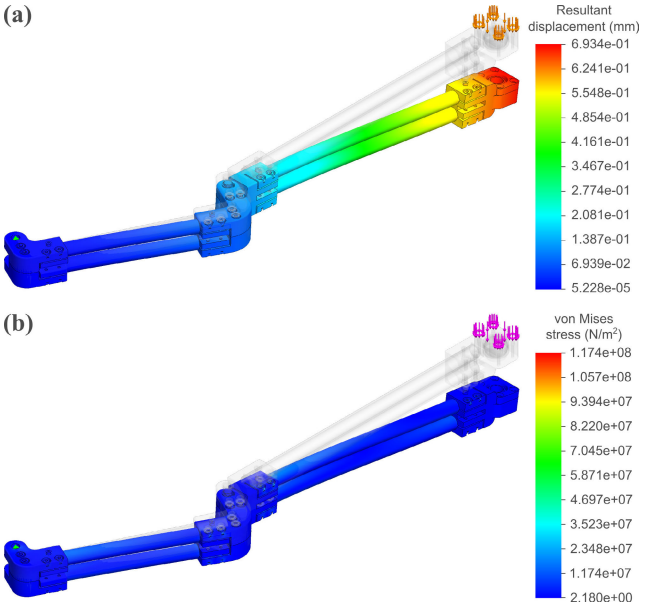

FIGURE 9. FEA result of the sweeping module: (a) the resultant displacement and (b) the von Mises stress.

The serial arm of the sweeping module was designed such that the top and bottom sides of the module are symmetrical; the base part of the serial arm can be detached from the crank link of the gravity compensation module (Fig. 7(b)). Thus, the prototype of the forearm assistance can be used for both right- and left- handed soldiers by simply changing the assembled configuration of the serial arm.

The interface for the mine-detection pole is depicted in Fig. 8. At the end-tip of the sweeping module, an interface is provided for connecting the mine-detection pole through the interface block. The interface block has a hollow-type ball joint. A connection plate with a cylinder-shape protrusion is attached at the bottom side of the mine-detection pole. Mine-detection pole is connected to the interface block by simply inserting the protrusion of the connection plate into the hole at the ball joint of the interface block. This structure enables the mine-detection pole to be easily detachable from the forearm assistance.

After the parameter optimization of the gravity compensation module, the stiffness coefficient of the linear spring was determined as 9,215.7 N/m. As depicted in Fig. 6, it is expected that within the range of $0° \leq \theta_1 \leq 39°$, the wearer must exert downward force to lower and manipulate the detection pole. Exerting suppressive force for manipulation may lead to inconvenience to the wearer. Because this range is the frequently-used range of motion during mine detection, a linear spring with lower stiffness, 6,040 N/m, was used instead to provide partial assistance. The load profile of the prototype with the linear spring is represented as a solid line with black color (Fig. 6). Within the practical range of motion, $0° \leq \theta_1 \leq 39°$, the average assistance rate is 76%. It is equivalent to holding and manipulating the detection pole

FIGURE 10. AX-Deminer forearm assistance worn by a mine-detection soldier.

with 1 kg of weight. Finally, the proposed forearm assistance worn by a soldier is depicted in Fig. 10.

V. EVALUATION

A. EXPERIMENT

The performance of the proposed forearm assistance was evaluated. Four training assistants for mine detection at the ROK Army Engineer School participated in this experiment. Participants were familiar with the textbook and had extensive experience teaching standard mine-detection postures to multiple trainees. Before the experiment, participants performed sufficient preliminary practice to simulate smooth mine detection operation while wearing the developed forearm assistance.

The experiment was conducted for the condition of wearing/un-wearing the prototype. Mine detection motion for the experiment was performed as follows. At the initial position, the mine detector is located at the wearer's center. First, the wearer slowly sweeps the pole to the right, and second, sweeps back toward the left side. Third, the pole returns to its initial position. Electromyogram (EMG) data obtained during this procedure were defined as the one-cycle of data. They conducted the experiment in random order with respect to the condition of wearing/un-wearing the forearm assistance; for each condition, the participant performed three cycles of the above procedure.

The muscle activity of the major muscles of the right upper arm—expected to receive significant load during mine detection—was measured to verify the performance of the proposed forearm assistance (Fig. 11). Muscle activity was analyzed by measuring EMG signals from the deltoid, biceps brachii, triceps brachii, and brachioradialis muscles of the right upper arm. The EMG data were measured with a sampling frequency of 1000 Hz and filtered with the 5th-order Butterworth low-pass filter with a 4 Hz cutoff frequency. The filtered EMG data were normalized based on maximum voluntary contraction (MVC) to reduce the influence of the participants.

FIGURE 11. Experimental setup for the evaluation of the AX-deminer. For observing muscle activities during mine detecting motion, EMG sensors were attached to major muscles of the upper arm: (1) deltoid, (2) biceps brachii, (3) triceps brachii, and (4) brachioradialis muscles.

B. EVALUATION RESULT

The experimental results are depicted in Fig. 12. Red and black lines represent mean values of EMG signals normalized by MVC for wearing and un-wearing the proposed forearm assistance, respectively. When the forearm assistance was not worn, the MVC of the deltoid, biceps brachii, triceps brachii, and brachioradialis muscles of the right upper arm were 25.6±5.9, 26.3±1.1, 48.9±0.5, and 66.7±4.7%MVC. When assisted by wearing the proposed forearm assistance, the MVC was 24.4±1.3, 9.1±0.6, 16.6±1.52, and 61.9±4.7%MVC. Whith the forearm assistance, muscle activity of upper arm muscles decreased by 1.8±2.2, 64.8±3.6, 66.0±2.7, and 7.0±0.8%, and the muscle activity of biceps brachii and triceps brachii muscles significantly decreased. The standard deviation of MVC also decreased while using the proposed forearm assistance.

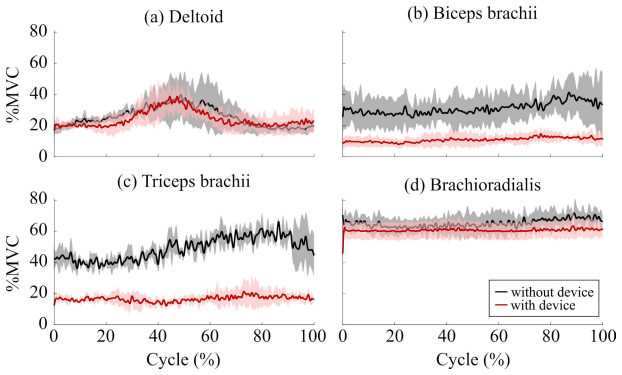

FIGURE 12. Experimental results: Mean values of EMG signals of four participants normalized by MVC. EMG signals were measured at (a) deltoid, (b) biceps brachii, (c) triceps brachii, and (d) brachioradialis muscles. Red and black lines represent mean values of the signals during mine detection motion *with* and *without* the proposed forearm assistance, respectively. Furthermore, one standard deviation of the signal is represented by the shaded area.

VI. CONCLUSION AND DISCUSSION

In this study, a novel concept of passive-type forearm assistance was suggested to compensate for the weight of a mine detector during the mine-detection operation of a soldier. The proposed forearm assistance was designed with a decoupled structure between sweeping and gravity

compensation modules to minimize the exposure of the mechanism to the wearer. The sweeping module was designed as a 2R-planar serial chain. It achieves the required range of the arm-sweeping motion; it transmits the detector's weight to the gravity compensation module. The gravity compensation module was designed using a planar six-bar linkage (crank-slider with one RR-dyad) with a linear spring. Because the gravity compensation unit is located at the wearer's back, the simple structure of the sweeping module is only exposed at the side of the wearer.

Design requirements were determined from motion analysis of two mine-detection soldiers. The amount of arm reach varies from 310 mm to 677 mm depending on working environments. Based on right-handed operating soldiers, the range of sweeping motion was measured to be 90.8° (or 32.2°) to the right (or left) side. Considering the elevation of the detection pole, it was lowered to 28.6° from the center of the pelvis; during the operation at an uphill slope, it was lifted to 3.0°.

Kinematic relationships were derived for sweeping and gravity compensation modules. Based on the kinematic relationships, the design parameters of the two modules were optimally synthesized to meet the design requirements. The prototype of the forearm assistance was designed using the results of parameter optimization. The design, which decoupled the sweeping module and the gravity compensation module, enabled independent parameter optimization of each module, leading to effective overall optimization. For the prototype design, the spring coefficient was further tuned by considering the comfort of the wearer.

Experimental validation of the prototype was performed against four mine-detection soldiers. Muscle activities of the right upper arm were measured for the deltoid, biceps brachii, triceps brachii, and brachioradialis muscles. Muscle activities of the biceps and triceps brachii significantly decreased to 64.8±3.6% and 66.0±2.7% in %MVC when the wearers performed the operation while wearing the prototype.

Because the bent arm is maintained during mine detection work, biceps brachii, a flexion muscle, is greatly activated [36], and simultaneously, isometric exercise is performed while holding a heavy mine detector and maintaining a bent arm. Thus, the triceps, which are opposite muscles of the biceps, are also activated to secure the stability of the joints [37]. Therefore, based on the results of the experiment, a significant decrease in muscle activity of the two muscles confirmed the effectiveness of the proposed forearm assistance. It is also expected from [38] that the proposed forearm assistance that reduces the muscle load of the mine-detection soldier may reduce the metabolic energy of the wearer.

This gravity compensation device has several limitations. It is specialized for assisting mine detectors, which may limit its applicability. When determining the target torque for the gravity compensation module, we considered only the operation of mine detectors. Specifically, it was designed for a specific model of mine detector. Different types of mine detectors may have variations in weight and motion patterns, potentially limiting the effectiveness of gravity compensation. However, if the operating range of the mine detector falls within the operational range of this device's sweeping module, it may be possible to apply this gravity compensation device by replacing the spring to accommodate the mine detector's weight.

Another limitation is that the device was validated for only four participants. However, the participants are experienced teaching assistants from the ROK Army Engineering School who have trained professionally mine-detection soldiers for a long time. Therefore, although it was verified with only four participants, the high reliability of the results can be guaranteed considering the participant's expertise. Furthermore, the validation was performed exclusively on flat ground. Considering that Korea's minefields are located predominantly in mountainous areas, the effectiveness in a real-world environment cannot be guaranteed as much as the verification results of this study. However, because the proposed forearm assistance was designed to operate and compensate for the detector's weight by considering the motion of human body joints under actual mountainous terrain, similar performance may be expected for detection operation in a real-world environment.

In this study, we have confirmed that the proposed gravity compensation device effectively assists mine detection soldiers. However, considering the study's limitations and future research directions, we anticipate several areas of further investigation. Future research will place a stronger emphasis on enhancing the operational efficiency and user-friendliness of the gravity compensation device for mine detection personnel. This includes considerations not only for mine detection tasks but also for other motions associated with detection task such as spraying on the ground and arm motion for calibrating the sensor of detection pole, as well as improvements in wearable comfort. Secondly, in the current version of the proposed forearm assistance, a ball joint was implemented to realize wrist motion of the wearer. The rotation center of the ball joint is apparently different from the wrist center of the wearer. The inconsistent center of motion may cause discomfort to the wearer when the soldier attempts to do fine adjustment of the detector's sensor plate. In order to resolve this, more study is needed to design the wrist structure with remote-center-of-rotation capability.

We anticipate potential improvements in the performance of mine detectors by implementing the proposed forearm assistance. Achieving enhanced mine detector performance requires high-spec sensors, although developing devices that soldiers can effectively employ in the field remains a challenging task. Nevertheless, the development of this gravity compensation device can extend the operational range of mine detectors, making valuable contributions to future research aimed at enhancing the accuracy and speed of mine detection. As a result, the development of this gravity compensation device opens up new possibilities for advancing mine detection operations.

REFERENCES

[1] E. J. Kim, "Toward an anthropology of landmines: Rogue infrastructure and military waste in the Korean DMZ," *Cultural Anthropol.*, vol. 31, no. 2, pp. 162–187, May 2016.

[2] M. K. Habib, "Mechanical mine clearance technologies and humanitarian demining: Applicability and effectiveness," in *Proc. 5th Int. Symp. Technol. Mine Problem*, Monterey, CA, USA, 2002, pp. 1–12.

[3] GICHD and Global CWD Repository. (2004). *A Study of Mechanical Application in Demining*. [Online]. Available: https://commons.lib.jmu.edu/cisr-globalcwd/190

[4] T. Theimer, "Summary report 910 mechanical clearance device," Global CWD Repository, Center Int. Stabilization Recovery, James Madison Univ., Harrisonburg, VA, USA, Tech. Rep. 1297, 2001. [Online]. Available: https://commons.lib.jmu.edu/cisr-globalcwd/1297

[5] O. Rolenec and M. Kopuletý, "Engineer devices for obstacle breaching in offensive operations and possibble application of engineer robots," in *Proc. Int. Conf. Mil. Technol. (ICMT)*, May 2017, pp. 200–206.

[6] M. A. Badrtdinov and D. V. Yudincev, "Automation of movement control for modern main tank T-90," *IOP Conf. Ser., Mater. Sci. Eng.*, vol. 966, no. 1, Nov. 2020, Art. no. 012115.

[7] T. Ueno, K. Amemiya, M. Ikuta, and O. Nishino, "Mine-clearing system for use in international peacekeeping," *Hitachi Rev.*, vol. 62, no. 3, pp. 224–228, 2013.

[8] P. Santana, J. Barata, H. Cruz, A. Mestre, J. Lisboa, and L. Flores, "A multi-robot system for landmine detection," in *Proc. IEEE Conf. Emerg. Technol. Factory Autom.*, vol. 1, Sep. 2005, pp. 721–728.

[9] K. Nonami, Q. Huang, D. Komizo, Y. Fukao, Y. Asai, Y. Shiraishi, M. Fujimoto, and Y. Ikedo, "Development of mine detection robot Comet-II and Comet-III," in *Proc. Int. Conf. Motion Vib. Control*. Tokyo, Japan: The Japan Society of Mechanical Engineers, 2002, pp. 449–454.

[10] P. G. D. Santos, E. Garcia, J. Estremera, and M. A. Armada, "DYLEMA: Using walking robots for landmine detection and location," *Int. J. Syst. Sci.*, vol. 36, no. 9, pp. 545–558, Jul. 2005.

[11] K. Kato and S. Hirose, "Development of the quadruped walking robot, TITAN-IX—Mechanical design concept and application for the humanitarian de-mining robot," *Adv. Robot.*, vol. 15, no. 2, pp. 191–204, Jan. 2001.

[12] J. D. Nicoud and M. K. Habib, "The Pemex-B autonomous demining robot: Perception and navigation strategies," in *Proc. IEEE/RSJ Int. Conf. Intell. Robots Syst. Hum. Robot Interact. Cooperat. Robots*, vol. 1, Aug. 1995, pp. 419–424.

[13] H. Najjaran and A. A. Goldenberg, "Landmine detection using an autonomous terrain-scanning robot," *Ind. Robot, Int. J.*, vol. 32, no. 3, pp. 240–247, Jun. 2005.

[14] M. A. Jaradat, M. N. BaniSalim, and F. H. Awad, "Autonomous navigation robot for landmine detection applications," in *Proc. 8th Int. Symp. Mechatronics Appl.*, Apr. 2012, pp. 1–5.

[15] Y. Ganesh, R. Raju, and R. Hegde, "Surveillance drone for landmine detection," in *Proc. Int. Conf. Adv. Comput. Commun. (ADCOM)*, Sep. 2015, pp. 33–38.

[16] P. Lucieer and J. L. Herder, "Design of an adjustable compensation mechanism for use in a passive arm support," in *Proc. Int. Design Eng. Tech. Conf. Comput. Inf. Eng. Conf.*, vol. 47446, 2005, pp. 491–500.

[17] G. Kramer, G. R. B. E. Romer, and H. J. A. Stuyt, "Design of a dynamic arm support (D_{AS}) for gravity compensation," in *Proc. IEEE 10th Int. Conf. Rehabil. Robot.*, Jun. 2007, pp. 1042–1048.

[18] (2020). *Saebomas Product Page*. [Online]. Available: https://www.saebo.com/shop/saebomas/

[19] B. E. Perry, E. K. Evans, and D. S. Stokic, "Weight compensation characteristics of Armeo Spring exoskeleton: Implications for clinical practice and research," *J. Neuroeng. Rehabil.*, vol. 14, no. 1, pp. 1–10, Dec. 2017.

[20] P. N. Kooren, A. G. Dunning, M. M. H. P. Janssen, J. Lobo-Prat, B. F. J. M. Koopman, M. I. Paalman, I. J. M. de Groot, and J. L. Herder, "Design and pilot validation of A-gear: A novel wearable dynamic arm support," *J. Neuroeng. Rehabil.*, vol. 12, no. 1, pp. 1–12, Dec. 2015.

[21] H.-M. Wang, D. K. L. Le, and W.-C. Lin, "Evaluation of a passive upper-limb exoskeleton applied to assist farming activities in fruit orchards," *Appl. Sci.*, vol. 11, no. 2, p. 757, Jan. 2021.

[22] M. Asgari, P. T. Hall, B. S. Moore, and D. L. Crouch, "Wearable shoulder exoskeleton with spring-cam mechanism for customizable, nonlinear gravity compensation," in *Proc. 42nd Annu. Int. Conf. IEEE Eng. Med. Biol. Soc. (EMBC)*, Jul. 2020, pp. 4926–4929.

[23] Y. Yamada, H. Arakawa, T. Watanabe, S. Fukuyama, R. Nishihama, I. Kikutani, and T. Nakamura, "Overhead work assist with passive gravity compensation mechanism and horizontal link mechanism for agriculture," in *Proc. 29th IEEE Int. Conf. Robot Hum. Interact. Commun. (RO-MAN)*, Aug. 2020, pp. 104–111.

[24] P. Maurice, J. Čamernik, D. Gorjan, B. Schirrmeister, J. Bornmann, L. Tagliapietra, C. Latella, D. Pucci, L. Fritzsche, S. Ivaldi, and J. Babič, "Objective and subjective effects of a passive exoskeleton on overhead work," *IEEE Trans. Neural Syst. Rehabil. Eng.*, vol. 28, no. 1, pp. 152–164, Jan. 2020.

[25] Ekso Bionics. (2020). *Ekso EVO Product Page*. [Online]. Available: https://eksobionics.com/ekso-evo/

[26] S. Spada, L. Ghibaudo, S. Gilotta, L. Gastaldi, and M. P. Cavatorta, "Investigation into the applicability of a passive upper-limb exoskeleton in automotive industry," *Proc. Manuf.*, vol. 11, pp. 1255–1262, Jan. 2017.

[27] A. Voilqué, J. Masood, J. C. Fauroux, L. Sabourin, and O. Guezet, "Industrial exoskeleton technology: Classification, structural analysis, and structural complexity indicator," in *Proc. Wearable Robot. Assoc. Conf. (WearRAcon)*, Mar. 2019, pp. 13–20.

[28] J. Theurel, K. Desbrosses, T. Roux, and A. Savescu, "Physiological consequences of using an upper limb exoskeleton during manual handling tasks," *Appl. Ergonom.*, vol. 67, pp. 211–217, Feb. 2018. [Online]. Available: https://www.sciencedirect.com/science/article/pii/S0003687017302296

[29] R. Altenburger, D. Scherly, and K. S. Stadler, "Design of a passive, ISO-elastic upper limb exoskeleton for gravity compensation," *ROBOMECH J.*, vol. 3, no. 1, pp. 1–7, Dec. 2016.

[30] K. Huysamen, T. Bosch, M. de Looze, K. S. Stadler, E. Graf, and L. W. O'Sullivan, "Evaluation of a passive exoskeleton for static upper limb activities," *Appl. Ergonom.*, vol. 70, pp. 148–155, Jul. 2018.

[31] S. Alabdulkarim and M. A. Nussbaum, "Influences of different exoskeleton designs and tool mass on physical demands and performance in a simulated overhead drilling task," *Appl. Ergonom.*, vol. 74, pp. 55–66, Jan. 2019. [Online]. Available: https://www.sciencedirect.com/science/article/pii/S0003687018302618

[32] G. W. Brown, "Equipment for use with hand held motion picture cameras," U.S. Patent 4 017 168, Apr. 12, 1977.

[33] J. Hull, R. Turner, and A. T. Asbeck, "Design and preliminary evaluation of two tool support arm exoskeletons with gravity compensation," *Mechanism Mach. Theory*, vol. 172, Jun. 2022, Art. no. 104802.

[34] C. Angeloni, P. O. Riley, and D. E. Krebs, "Frequency content of whole body gait kinematic data," *IEEE Trans. Rehabil. Eng.*, vol. 2, no. 1, pp. 40–46, Mar. 1994.

[35] J. Duffy, *Statics and Kinematics With Applications to Robotics*. Cambridge, U.K.: Cambridge Univ. Press, 1996.

[36] E. Nygaard, M. Houston, Y. Suzuki, K. Jørgensen, and B. Saltin, "Morphology of the brachial biceps muscle and elbow flexion in man," *Acta Physiol. Scand.*, vol. 117, no. 2, pp. 287–292, Feb. 1983.

[37] P. L. Gribble, L. I. Mullin, N. Cothros, and A. Mattar, "Role of cocontraction in arm movement accuracy," *J. Neurophysiology*, vol. 89, no. 5, pp. 2396–2405, May 2003.

[38] E. Homsher and C. J. Kean, "Skeletal muscle energetics and metabolism," *Annu. Rev. Physiol.*, vol. 40, no. 1, pp. 93–131, Mar. 1978.

MYUNGHYUN LEE received the B.S. degree in physics and the M.S. and Ph.D. degrees in mechanical engineering from the Korea Advanced Institute of Science and Technology (KAIST), Daejeon, Republic of Korea, in 2009, 2011, and 2020, respectively.

She is currently a Researcher with Agency for Defense Development, Daejeon. Her research interests include biomechanics, human gait, and wearable robot design.

YONGCHEOL KIM received Ph.D. degrees in mechanical engineering from Chung-Ang University, Seoul, Republic of Korea, in 2019.

Since 2019, he has been a Senior Researcher with Agency for Defense Development, Daejeon, Republic of Korea. His research interests include musculoskeletal dynamics and wearable robot design.

GWANG TAE KIM received the M.S. degree in electrical engineering from the Korea Advanced Institute of Science and Technology (KAIST), Daejeon, Republic of Korea, in 2014.

He is currently a Senior Researcher with Agency for Defense Development, Daejeon. His primary research interests include gait analysis and wearable robot control.

SANG HUN JOO received the B.S. degree in mechanical engineering from the Pohang University of Science and Technology (POSTECH), Pohang, Republic of Korea, in 2019.

From 2019 to 2022, he was an active-duty assignment with Agency for Defense Development, Daejeon, Republic of Korea. His research interest includes wearable robot design.

MAN BOK HONG received the B.S. degree in mechanical engineering from Hongik University, Seoul, Republic of Korea, in 1998, and the M.S. and Ph.D. degrees in mechanical engineering from Yonsei University, Seoul, in 2003 and 2009, respectively.

From 2009 to 2011, he was a Postdoctoral Researcher with the Biomedical Engineering Branch, Division of Convergence Technology, National Cancer Center, Gyeonggi-do, Republic of Korea, and from 2011 to 2013, he was a Postdoctoral Fellow with the Interaction and Robotics Research Center, National Agenda Research Division, Korea Institute of Science and Technology, Seoul. He is currently a Principal Researcher with the first Ground Weapon Systems PMO—Ground Technology Research Institute, Agency for Defense Development, Daejeon, Republic of Korea. His current research interests include the kinematic geometry of robot mechanisms on the basis of the theory of screws, the synthesis of robot compliance, the design of surgery robot systems, and the design and compliant control of power assistant exoskeletons.